Photodriven Electron Transport within the Columnar Perylenediimide Nanostructures Self-Assembled with Sulfonated Porphyrins in Water

ARTICLE *in* THE JOURNAL OF PHYSICAL CHEMISTRY C · OCTOBER 2012

Impact Factor: 4.77 · DOI: 10.1021/jp308549w

2 AUTHORS, INCLUDING:

Mustafa Supur
University of Alberta
20 PUBLICATIONS **226** CITATIONS

SEE PROFILE

THE JOURNAL OF PHYSICAL CHEMISTRY C

Article

pubs.acs.org/JPCC

Photodriven Electron Transport within the Columnar Perylenediimide Nanostructures Self-Assembled with Sulfonated Porphyrins in Water

Mustafa Supur[†] and Shunichi Fukuzumi*[,†,‡]

[†]Department of Material and Life Science, Graduate School of Engineering, Osaka University, ALCA, Japan Science and Technology Agency (JST), Suita, Osaka 565-0871, Japan

[‡]Department of Bioinspired Science, Ewha Womans University, Seoul 120-750, Korea

Supporting Information

ABSTRACT: Columnar stacks of *N*,*N*′-di(2-(trimethylammoniumiodide)ethylene) perylenediimide (TAIPDI)$_n$ can host *meso*-tetrakis(4-sulfonatophenyl)porphyrin zinc tetrapotassium salt (ZnTPPSK$_4$) molecules at different ratios through the ionic and $\pi-\pi$ interactions prompted by an aqueous environment. Photoexcitation of this host–guest complex generates very fast charge separation (1.4×10^{12} s^{-1}). Charge recombination is markedly decelerated by a probable electron delocalization mechanism along the long-range of tightly stacked TAIPDIs (4.6×10^{8} s^{-1}), giving an exceptional k_{CS}/k_{CR} ratio of 3000 as determined by using time-resolved transient absorption techniques.

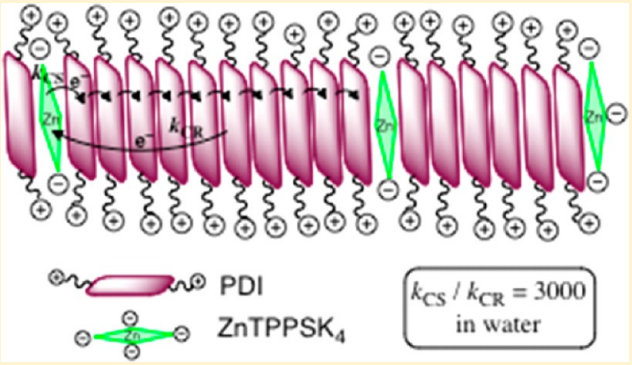

1. INTRODUCTION

Charge separation is an essential process to convert solar energy into a chemical potential in the photosynthesis[1] and in the organic photovoltaic cells as well.[2] In the natural system, this process has been realized by utilizing a series of redox-active units meticulously aligned to transfer the electron to the next component until a distance to restrain the fast charge recombination is adequately reached. The charge separation distance between the primary electron donor, P680, and the electron-accepting plastoquinone Q_A ($P680^{\bullet+}Q_A^{\bullet-}$) in the photosynthetic reaction center of the cyanobacterial photosystem II is approximately 3.4 nm.[3] A number of photosynthetic reaction center mimicries have been so far developed,[4] extending the distances for charge separation up to 5.0 nm.[5] Assuming that such a distance is applicable for transporting the charge carriers (electron and hole) to the opposite electrodes in a solar cell, collecting the solar photons by a layer of this length will be insufficient because it is known that the active layers of current organic photovoltaic cells (bilayer or bulk heterojunction) require the thickness of at least 100 nm for efficient light harvesting if the organic materials, having high absorption coefficients (10^5 cm^{-1}), are used.[2b,6,7] Taking the inevitable loss of the excitation energy at each step of electron transfer in natural and artificial systems into account,[4c] elongation of the charge separation distance by this strategy is not practical, because of the synthetic difficulties to fabricate multicomponent molecular arrays and additional light harvesting systems. Control of the molecular alignment of such complex systems at microscopic scale is another obstacle to deal with.

π-Conjugated polymers, on the other hand, have been extensively preferred for transporting the photogenerated charges throughout long distances within the active layer to obtain an electron flow.[8,9] Recently, Friend et al.[10] explained this long-range charge transport within the bulk heterojunction cells of such polymers through the presence of the charge delocalization. Delocalized states of π-electron systems were reported to enable the charges to override the Coulombic interactions and fast charge recombination, thereby enhancing the external quantum efficiencies. Extensive charge delocalization[11] and its effect on stabilizing the electron transfer products, i.e., radical cation and anion, against the charge recombination[12] have been investigated in dimer, oligomer, and polymer systems in solution.

In addition to π-delocalization, molecular orientation in one dimension at nanoscale is of importance to boost the device efficiency.[13] In this regard, the self-assemblies of perylenediimide (PDI) dyes, forming one-dimensional nanostructures, have drawn much attention.[14] An average length of PDI nanofibrils was reported to reach about 0.3 mm in a study,[15] exhibiting the effect of the strong $\pi-\pi$ stacking in one dimension. Long axes of such molecular architectures of PDI exhibit electron hopping due to π-electron delocalization within

Received: August 28, 2012
Revised: October 15, 2012
Published: October 22, 2012

   dx.doi.org/10.1021/jp308549w | *J. Phys. Chem. C* 2012, 116, 23274–23282

the stacks when exposed to a reducing agent or n-dopant.[16] Electron migration in one dimension via π-delocalization can be accessed by light in the presence of a photoactive electron donor.[17] There are only a few studies of one-dimensional self-assemblies of PDI, examining the electron transport within the π-stacks.[18] Such self-assemblies were, however, mostly constructed in nonpolar solvents.

In this study, the formation and the photoinitiated electron-transfer process of a self-assembly of *N*,*N*′-di(2-(trimethylammonium iodide)ethylene)perylenediimide (TAIPDI) and *meso*-tetrakis(4-sulfonatophenyl)porphyrin zinc tetrapotassium salt ($ZnTPPSK_4$) have been investigated in water, for the first time (Figure 1). An aqueous medium is of choice because it provokes the self-assembly of such highly extensive π-systems[19] without any other additional treatment; moreover, it facilitates the electron-transfer processes due to high polarity.[20] TAIPDI molecules undergo π-stacking [$(TAIPDI)_n$] in water, resulting in one-dimensional nanostructures.[21] Apart from solubilizing the TAIPDI stacks in water, cationic trimethylammonium heads also enhance the ionic interactions with water-soluble $ZnTPPSK_4$, bearing anionic sulfonic groups. By this way, ionic interactions strongly support the hydrophobic interactions between the aromatic cores of TAIPDI and $ZnTPPSK_4$, thereby yielding robust and adjustable donor−acceptor self-assemblies, which seem suitable conduits for photodriven charge transport in an aqueous medium.

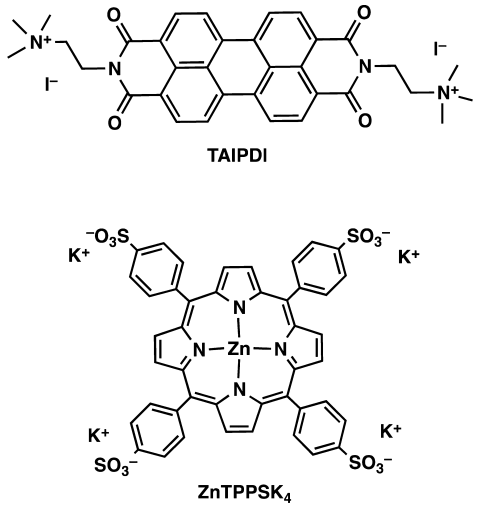

Figure 1. Molecular structures of the components used in this study.

2. EXPERIMENTAL SECTION

2.1. Materials. *N*,*N*′-di(2-(trimethylammoniumiodide)-ethylene)perylenediimide (TAIPDI) was synthesized according to reported procedures.[21,22] *Meso*-tetrakis(4-sulfonatophenyl)-porphyrin zinc tetrapotassium salt ($ZnTPPSK_4$) was prepared from commercially available *meso*-tetrakis(4-sulfonatophenyl)-porphyrin (TPPS).[23] Purification of water (18.2 Ω cm) was performed with a Milli-Q system (Millipore, Direct-Q 3 UV).

2.2. Instruments. Steady-state absorption measurements were recorded on a Hewlett-Packard 8453 diode array spectrophotometer. Fluorescence measurements were carried out on a Shimadzu spectrofluorophotometer (RF-5300PC). Measurements of emission quantum yields were carried out on a Hamamatsu C9920-0X(PMA-12) U6039-05 fluorescence spectrofluorometer with an integrating sphere adapted to a right angle configuration at room temperature. Dynamic light scattering (DLS) measurements were done by using a Zetasizer Nano S instrument (Malvern Instruments Ltd., Malvern, U.K.). The DLS instrument used in this work has a range between 0.6

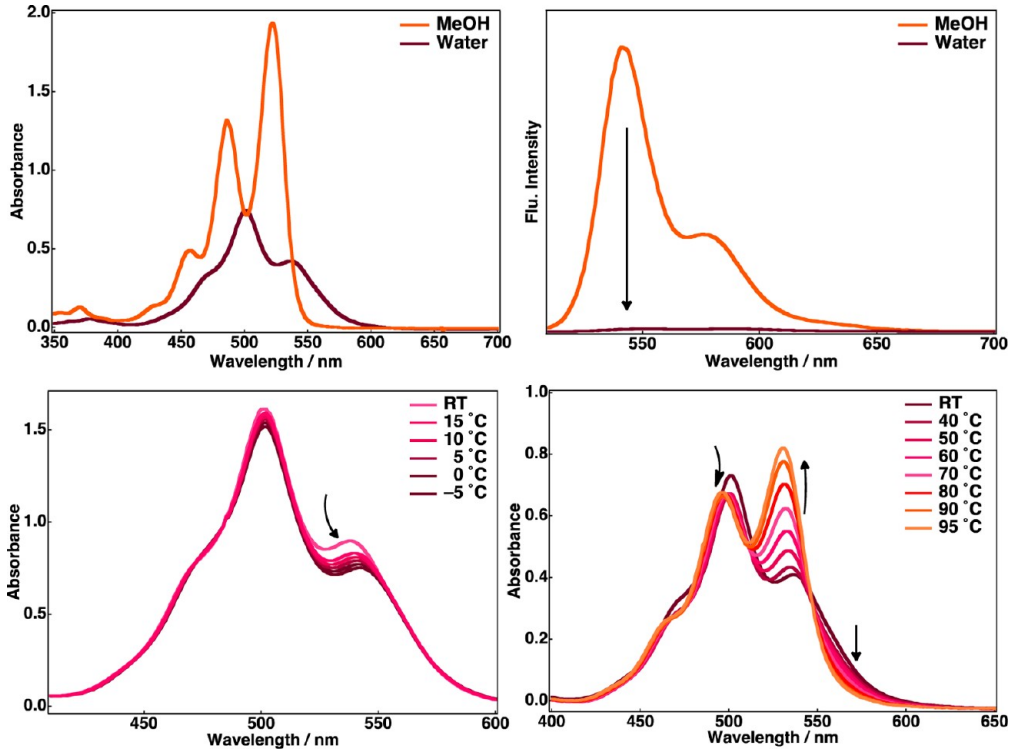

Figure 2. Upper panel: Steady-state absorption spectra of 0.02 mM TAIPDI (left) and emission spectra of 0.08 mM TAIPDI (right) in water and MeOH (λ_{exc} = 500 nm). Lower panel: Steady-state absorption spectra of TAIPDI upon cooling (left) and heating (right) in water.

dx.doi.org/10.1021/jp308549w | J. Phys. Chem. C 2012, 116, 23274−23282

and 6000 nm; therefore, any structures over this limit could not be detected. Electrochemical measurements were performed on an ALS630B or ALS730D electrochemical analyzer in deaerated water containing 0.10 M Na_2SO_4 as supporting electrolyte. A conventional three-electrode cell was used with a platinum working electrode (surface area of 0.3 mm^2) and a platinum wire as the counter electrode. The Pt working electrode was routinely polished with ALS polishing alumina suspension (0.05 μm) and rinsed with water and acetone before use. The measured potentials were recorded with respect to a saturated calomel electrode (SCE). All electrochemical measurements were carried out under an atmospheric pressure of N_2. Scanning electron microscopy (SEM) images were taken on a JEOL FE-SEM JSM-6701F instrument operating at 5 kV. Time-resolved fluorescence was measured by Horiba Scientific TCSPC on FluoroMax-4 spectrofluorophotometer. A pulsed diode light source (Horiba Scientific NanoLED) was used for excitation at 488 nm with a repetition rate up to 1 MHz (pulse width 1.3 ns). The emission detector is an R928P for high sensitivity in photon-counting mode (180−850 nm). Femtosecond transient absorption spectroscopy experiments were conducted using an ultrafast source, Integra-C (Quantronix Corp.), an optical parametric amplifier, TOPAS (Light Conversion Ltd.), and a commercially available optical detection system, Helios provided by Ultrafast Systems LLC. The source for the pump and probe pulses was derived from the fundamental output of Integra-C (780 nm, 2 mJ per pulse, and fwhm = 130 fs) at a repetition rate of 1 kHz. 75% of the fundamental output of the laser was introduced into TOPAS, which has optical frequency mixers resulting in a tunable range from 285 to 1660 nm, while the rest of the output was used for white light generation. Typically, 2500 excitation pulses were averaged for 5 s to obtain the transient spectrum at a set delay time. Kinetic traces at appropriate wavelengths were assembled from the time-resolved spectral data. All measurements were conducted at 298 K. For nanosecond transient absorption measurements, deaerated solutions of the compounds were excited with a Panther optical parametric oscillator (OPO) equipped with a Nd:YAG laser (Continuum, SLII-10, fwhm = 4−6 ns) with a power of 10−15 mJ per pulse. The photochemical reactions were monitored by continuous exposure to a Xe lamp (150 W) as a probe light and a detector (SpectraPro 300i). The transient spectra were recorded using fresh solutions in each laser excitation. Solutions were deoxygenated by N_2 purging for about 15 min prior to the all transient spectral measurements.

3. RESULTS AND DISCUSSION

3.1. Characterization of TAIPDI in Solution and Solid State. TAIPDI dissolves in methanol (MeOH) as the representative 0−0, 0−1, 0−2, and 0−3 transitions of typical PDI are clearly observed at 522, 486, 457, and 429 nm, respectively (Figure 2). TAIPDI molecules, on the other hand, assemble into stacks in water via strong $\pi-\pi$ interactions of hydrophobic aromatic cores. Solubilized by polar trimethylammonium heads in water, these π-stacks give absorption peaks at 537 and 501 nm with a shoulder around 470 nm. Due to high solubility of TAIPDI stacks in water, high absorption coefficients (ε = 37 500 M^{-1} cm^{-1} for 0.02 mM at 501 nm) are observed, comparable to its monomer form (ε = 97 200 M^{-1} cm^{-1} at 522 nm) in MeOH. In contrast, dispersed PDI aggregates usually have low absorption due to low solubility.[17,24] The 4-fold increase in concentration of TAIPDI causes 2 nm of red shift of the peak at 537 nm (Figure S1, Supporting Information). Temperature dependence of aggregation in water has also been tested (Figure 2). Cooling does not cause any shift at 501 nm; however, a meaningful red shift is observed at 537 to 543 nm, which means the energy separation between two absorption peaks becomes greater. Thus, it can be concluded that high concentration or low temperature result in closer cofacial order of TAIPDI chromophores as the exciton coupling grows stronger.[25] The increase in the temperature causes apparent decomposition of aggregation as the vibrational transitions at 531 (0−0), 496 (0−1), and 465 nm (0−2) have been restored. Nonetheless, the lower ratio of 0−0 transition to 0−1 transition (1.21) in water at 95 °C than that in MeOH at room temperature (1.48) indicates that π-stacking is still present even at such a high temperature, emphasizing the effect of an aqueous environment on aromatic $\pi-\pi$ interactions.[22]

Vibrationally resolved emission of TAIPDI in MeOH appears at 540 and 577 nm with high quantum efficiency. On the other hand, the fluorescence emission is drastically ceased by $\pi-\pi$ electronic coupling in water (Figure 2 and Table 1).[26]

Table 1. Absolute Fluorescence Quantum Yields (Φ_f) and Aggregation Yields of TAIPDI at Different Concentrations in Water

concentration (mM)	Φ_f	aggregation yield
0.02[a]	0.059	0.92
0.05	0.028	0.96
0.08	0.014	0.98
0.15	0.008	0.99

[a]Φ_f of 0.02 mM TAIPDI is 0.70 in MeOH.

Fluorescence quenching becomes notable as the concentration increases. Weak emission of TAIPDI stacks (0.02 mM) in water is detected at 548 and 585 nm, which are red-shifted compared to that in MeOH. The emission spectrum of 0.33 mM TAIPDI gives a maximum at 595 nm with a less intense peak at 549 nm, which in fact shows a reflection of its absorption spectrum in water (Figure S1, Supporting Information). This mirror-imaged emission results from face-to-face arrangement of the TAIPDI molecules, whose transition dipoles are parallel.[27] Aggregation yields can be approximated from the emission quenching at different concentrations (Table 1).[28]

The radical anion of TAIPDI stacks [$(TAIPDI)_n^{\bullet-}$], generated by using water-soluble hydrazine as a strong electron donor, gives absorption at 730, 817, and 985 nm in water (Figure S2, Supporting Information).[29] Compared to the radical anion of monomer PDIs, the absorption spectra of $(TAIPDI)_n^{\bullet-}$ are broader and red-shifted due to probable electron delocalization within the π-stacks of TAIPDI.[29,30] Such broadening has also been observed in the oligomeric self-assemblies of PDI.[31] $(TAIPDI)_n^{\bullet-}$ is quite stable in deaerated water for a few weeks.

The size distribution of TAIPDI aggregates in water was examined by dynamic light scattering (DLS) measurements. The DLS diagram of TAIPDI aggregates reveals a size distribution ranging from 105 to 460 nm, with a mean size of 188 nm (Figure S3, Supporting Information).[32]

The effect of π-stacking in water on the excited-state dynamics of TAIPDI has been examined in comparison with those of its monomer in MeOH by using femtosecond transient absorption spectroscopy. As shown in Figure 3, the transient spectra of monomeric TAIPDI in MeOH display mirror-

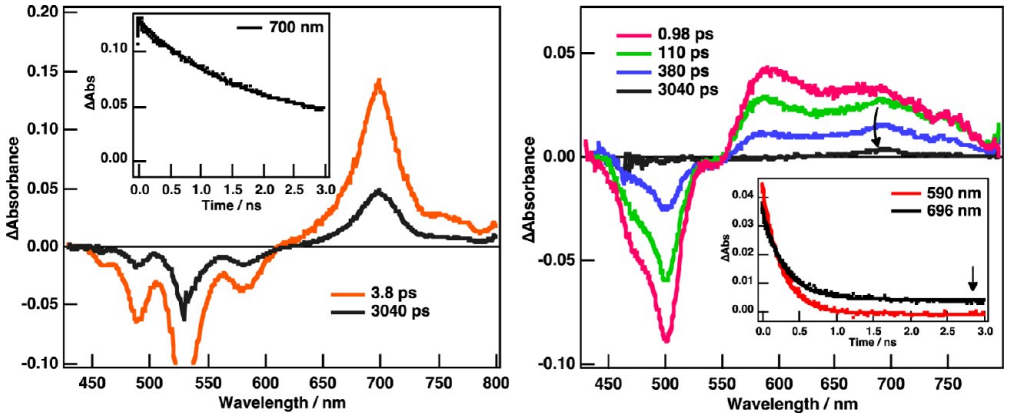

Figure 3. Femtosecond transient absorption spectra of 0.05 mM TAIPDI in MeOH (left) and in water (right) at indicated time delays (λ_{exc} = 390 nm). Insets: Time profiles at corresponding wavelengths.

imaged bleaching from 440 to 600 nm, which corresponds to ground state absorption and stimulated emission. The positive transient absorption centered at 700 nm is the attribute of singlet-excited states of TAIPDI molecules. The lifetime of singlet-excited state is determined from time-resolved fluorescence measurements as 4.4 ns (Figure S4, Supporting Information). All transient features and lifetime values are in agreement with the previously reported data.[33] On the other hand, TAIPDI stacks (0.05 mM) in water reveal intense bleaching at 501 nm with a negative shoulder at 470 nm (Figure 3). Small negative absorption is also recognized at around 540 nm. These traits correspond to ground state absorption of TAIPDI in water. Stimulated emission was not observed due to quenching. Besides, transient maxima at 590 nm and another absorption band centered at 696 nm emerge as broad positive features reaching the end of the spectral window. These traits are assigned to the singlet-excited states of $(TAIPDI)_n$. As the time elapses, the peak at 590 nm decays faster than that at 696 nm and the small positive signal at around 700 nm remains persistent. The decay profile at 590 nm affords a lifetime of 263 ps (3.8×10^9 s^{-1}), coinciding with that of bleaching at 501 nm (270 ps). 88% of the absorption band at 696 nm decays with a lifetime of 303 ps (3.3×10^9 s^{-1}), and 12% survives within the time course of the femtosecond measurements. At higher concentration (0.13 mM), the decays at 590 and 696 nm give lifetimes of 220 ps (4.5×10^9 s^{-1}) and 235 ps (4.3×10^9 s^{-1}), respectively, shorter than former lifetime values (Figure S5, Supporting Information). This time, 96% of the decay is completed at around 700 nm. These values are quite consistent with the aggregation yields (Table 1). The fluorescence lifetime measurements of TAIPDI in water afford a lifetime of 5.0 ns, which is probably the trace of this remaining portion (Figure S6, Supporting Information). The long-lived transient trait at around 700 nm seems like inheritance from unstacked TAIPDI present in water. In conclusion, the singlet-excited state lifetimes of TAIPDI in water are concentration dependent. Although the lifetime values are shorter compared to their monomeric form, they seem still usable for supramolecular photoinduced processes.

The stacking behavior of TAIPDI in the solid form has been displayed by using scanning electron microscopy (SEM). Extensive π-stacking results in a one-dimensional morphology, as shown in SEM images (Figure 4).[34] The columnar structures are about 100−150 nm in width, and the average length is in micrometer scale ranging from 1 to 10 μm. Nanostructures of

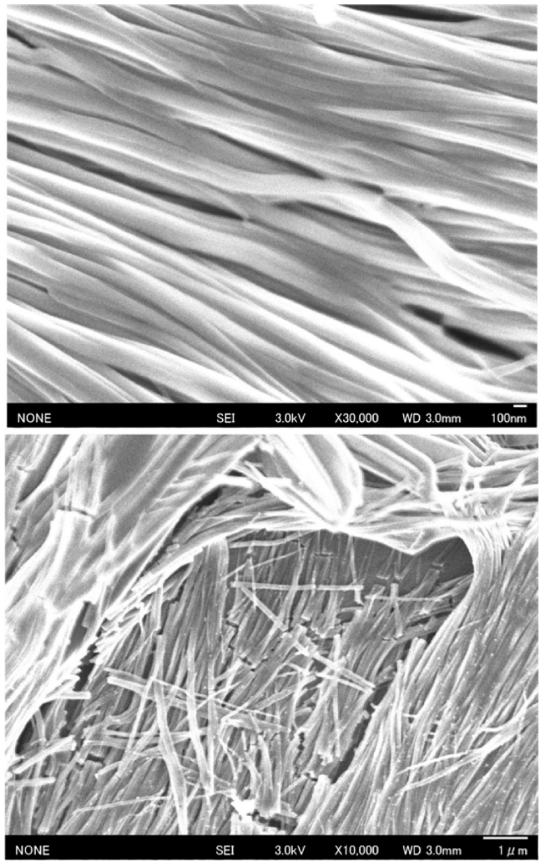

Figure 4. SEM images of nanostructures of TAIPDI obtained from its aqueous solution.

TAIPDI seem brittle, thereby decreasing the average length. The aspect ratio of these structures (length/width) is over 40. PDIs, having linear side-chains, generally tend to reveal one-dimensional morphologies in aggregation.[35] Linear ethylene chains of TAIPDI may have a controlling effect on this columnar stacking. Compared to other nanostructures of PDIs, bearing longer side-chains,[17] those of TAIPDI have a narrower average width probably due to the electrostatic repulsion of positively charged trimethylammonium heads.

3.2. Formation of Self-Assemblies of $(TAIPDI)_n$ and $ZnTPPSK_4$ in Water. Assembly formation between the TAIPDI stacks and water-soluble $ZnTPPSK_4$ has been

dx.doi.org/10.1021/jp308549w | J. Phys. Chem. C 2012, 116, 23274−23282

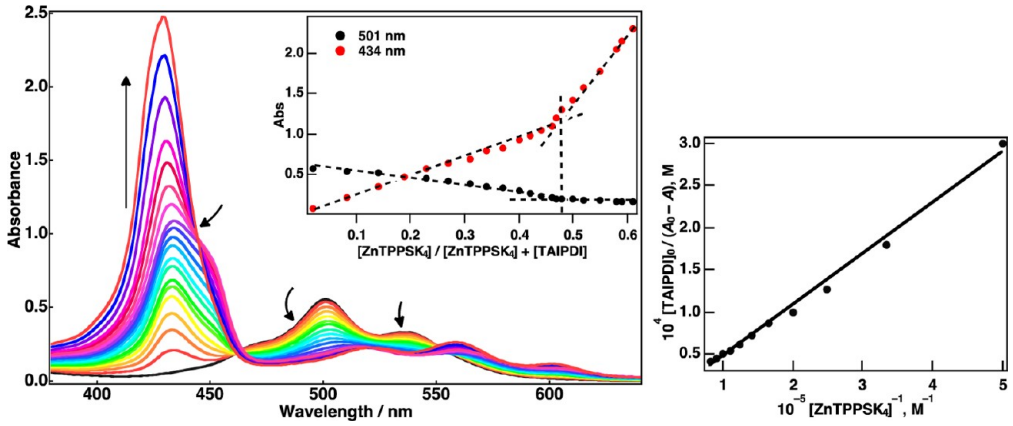

Figure 5. Absorption spectral changes during the titration of TAIPDI with $ZnTPPSK_4$ in water. Inset: Plots of absorbance vs ($[ZnTPPSK_4]$/$[ZnTPPSK_4]$ + [TAIPDI]) showing the stoichiometry of the complex at indicated wavelengths (left). Linear plot of $[TAIPDI]_0/(A - A_0)$ vs $[ZnTPPSK_4]^{-1}$ at 501 nm to evaluate the binding constant (right).

examined by steady-state absorption and emission spectroscopy and confirmed by DLS measurements. Upon addition of $ZnTPPSK_4$, the absorption features of $(TAIPDI)_n$ decline gradually, while a red shift from 501 to 515 nm takes place (Figure 5). A new absorption band in regard to $ZnTPPSK_4$ evolves at 434 nm with a shoulder at around 450 nm. Additionally, the small rise at 559 and 601 nm is noticeable. $ZnTPPSK_4$ normally gives a sharp Soret peak at 422 nm with the Q-bands at 556 and 595 nm in water (Figure S7, Supporting Information). As studied previously, ionic interactions cause only a few nm of red shift of the Soret of $ZnTPPSK_4$ without any decrease or broadening.[36] Thus, markedly different characteristics of new absorption spectra of the TAIPDI−$ZnTPPSK_4$ complex compared to those of its components indicate that the self-assembly has been established not only by ionic interactions but also by strong $\pi-\pi$ interactions between the aromatic cores of TAIPDI and $ZnTPPSK_4$. To determine the stoichiometry of the complex, absorbance change at 434 and 501 nm versus the molar ratio of added $ZnTPPSK_4$ to the total concentration has been followed. Both plots of these wavelengths revealed breaks coinciding at ca. 0.47, indicating a 1:1 stoichiometry between TAIPDI and $ZnTPPSK_4$ (Scheme 1). It is worth noting that the ratio given

Scheme 1

$$\text{TAIPDI} + \text{ZnTPPSK}_4 \underset{}{\overset{K_0}{\rightleftharpoons}} \text{TAIPDI–ZnTPPSK}_4$$

does not mean that TAIPDI and $ZnTPPSK_4$ form individual 1:1 complexes in the water. This notion describes the number of the components present within the polymeric π-stacks assembled via ionic and $\pi-\pi$ interactions.

From the slope of the linear plot in Figure 5, the formation constant (K_0) of TAIPDI−$ZnTPPSK_4$ was determined to be 1.0×10^5 M^{-1}.[37,38] After the 1:1 ratio exceeded by the addition of $ZnTPPSK_4$, a new isosbestic point emerges at 444 nm, while the shoulder around 450 nm disappears and the absorption band at 434 nm rises with a blue shift to 429 nm probably due to penetration of more $ZnTPPSK_4$ molecules into TAIPDI stacks with a new stoichiometry.

$ZnTPPSK_4$ has been titrated with TAIPDI as well. During the titration, the Soret of $ZnTPPSK_4$ at 422 nm decreases regularly, being replaced with another peak at 430 nm, as the isosbestic point appears at 428 nm (Figure 6). While the absorbance at 430 nm reaches its climax, the molar ratio of TAIPDI to the total concentration marks a value around 0.4 (Figure 6, inset), implying a ratio of 2:3 between TAIPDI and $ZnTPPSK_4$ molecules within the stacks (Scheme 2). At this ratio, absorption characteristics of the complex seem almost identical to those of the complex formed by the addition of excess $ZnTPPSK_4$ in the former titration of $(TAIPDI)_n$ (Figure 5). This ratio may indicate the saturated state of TAIPDI stacks with $ZnTPPSK_4$ molecules. As the titration continues, the second isosbestic point appears at 444 nm, as observed in the former titration. Accordingly, the maximum at 430 nm reduces with a slight red shift to 434 nm, while a broad shoulder ascends around 450 nm. The Q-bands of $ZnTPPSK_4$ also reveal a bathochromic shift. On the other hand, TAIPDI absorbs broadly at around 516 nm. Absorbance plots at 422, 430, and 520 nm properly give breaks at ~0.5 in the inset of Figure 6. All the absorption features at this ratio are the same as those of 1:1 assembly in Figure 5 (Scheme 2). The decrease at 430 nm yields a linear plot according to Scheme 2. From the slope of this linear correlation (Figure 6), the formation constant (K_2) of TAIPDI−$ZnTPPSK_4$ was determined to be 6.4×10^4 M^{-1}, which is quite close to K_0.[39] Further addition of TAIPDI does not change the absorption traits of the complex except for the rise at around 500 nm, resulting from free TAIPDI stacks.[40]

Titration of $ZnTPPSK_4$ with TAIPDI stacks also leads to fluorescence quenching, most probably due to intramolecular photoinduced electron transfer. $ZnTPPSK_4$ fluoresces with a maximum at 604 nm.[36] Gradual decrease of this emission by the addition of TAIPDI is observed as the TAIPDI−$ZnTPPSK_4$ complex is eventually constructed with a formation constant (1.1×10^6 M^{-1})[38] comparable to the K_0 (Figure 7).

DLS measurements display an average size distribution of 1085 nm for the TAIPDI−$ZnTPPSK_4$ complex (Figure S8, Supporting Information), which is significantly higher than that of TAIPDI itself. Strong $\pi-\pi$ interactions together with the ionic interactions may cause growing size of the self-assemblies in water.

To conclude, strong noncovalent interactions between TAIPDI and $ZnTPPSK_4$ represent versatile complex motifs as understood from the titrations.

3.3. Photoinduced Electron Transfer Dynamics. The free energy values for supramolecular photoinduced charge separation (ΔG_{CS}) between TAIPDI and $ZnTPPSK_4$ in water have been calculated according to the equation below:[41]

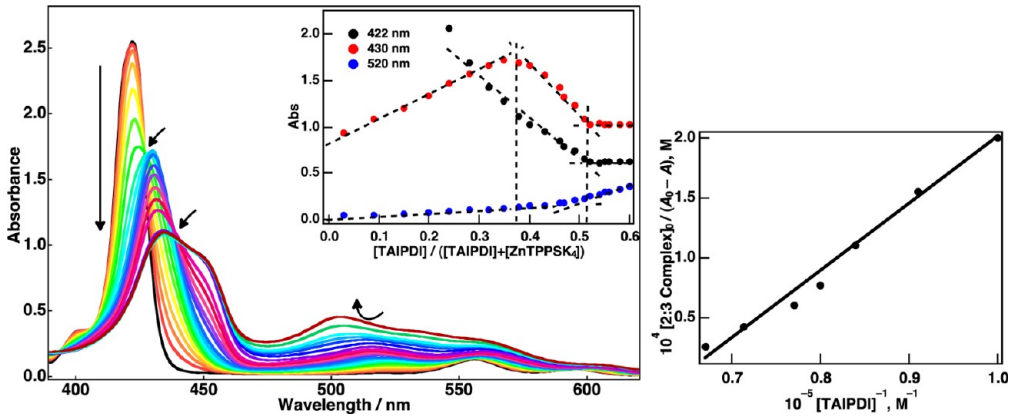

Figure 6. Absorption spectral changes during the titration of $ZnTPPSK_4$ with TAIPDI in water. Inset: Plots of absorbance vs ([TAIPDI]/[TAIPDI] + [$ZnTPPSK_4$]) showing the stoichiometry of the complex at indicated wavelengths (left). Plot of $[2:3\ complex]_0/(A - A_0)$ vs $[TAIPDI]^{-1}$ at 430 nm to evaluate the binding constant (right).

Scheme 2

$$TAIPDI_2 + 3ZnTPPSK_4 \underset{}{\overset{K_1}{\rightleftharpoons}} TAIPDI_2{-}(ZnTPPSK_4)_3$$

$$TAIPDI_2{-}(ZnTPPSK_4)_3 + TAIPDI \overset{K_2}{\rightleftharpoons} TAIPDI_3{-}(ZnTPPSK_4)_3$$

or

$$TAIPDI_2{-}(ZnTPPSK_4)_3 + TAIPDI \overset{K_2}{\rightleftharpoons} (TAIPDI{-}ZnTPPSK_4)_3$$

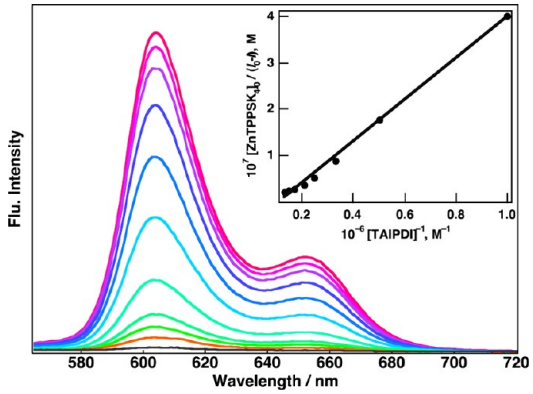

Figure 7. Emission spectral changes during the titration of $ZnTPPSK_4$ with TAIPDI in water. Inset: Plot of $[ZnTPPSK_4]_0/(I - I_0)$ vs $[TAIPDI]^{-1}$ at 604 nm to evaluate the binding constant.

$$\Delta G_{CS} = e(E_{ox} - E_{red}) - \Delta E_S + \Delta G_s$$

where E_{ox} is the first one-electron oxidation potential of $ZnTPPSK_4$, E_{red} is the first one-electron reduction potential of TAIPDI, ΔE_S is the lowest excited state energy of $ZnTPPSK_4$ or TAIPDI stacks, and ΔG_s is the static Coulomb energy in water.[42] E_{ox} for $ZnTPPSK_4$ and E_{red} for TAIPDI have been determined as 0.58 and −0.25 V vs SCE in water containing 0.10 M Na_2SO_4, respectively, by using cyclic and differential pulse voltammetry (Figure S9, Supporting Information). If the $ZnTPPSK_4$ is considered as a photosensitizer with a ΔE_S value of 2.07 eV estimated from its absorption and fluorescence emission,[38b] then the driving force for charge separation is estimated to be 1.24 eV. Despite the π-stacking, the driving force for charge separation via the excited states of $(TAIPDI)_n$, having sufficient lifetimes for close interactions, is not out of the question (vide supra). Moreover, one-dimensional morphology facilitates the exciton migration, which can eventually produce charge separation.[36,43] Excitation of $(TAIPDI)_n$ can generate a driving force for charge separation of 1.49 eV, as determined from the absorption and weak emission spectra at different concentrations (2.32 eV). Water, as an extremely polar ambience, has an important role for highly exothermic driving forces.

The photoinduced processes taking place within the TAIPDI−$ZnTPPSK_4$ self-assembly have been monitored by using femtosecond and nanosecond transient spectroscopy. A careful balance between obtaining the highest absorption at the excitation wavelength and permitting the maximum electron delocalization within the π-stacks of TAIPDI required mixing 1 equiv of $ZnTPPSK_4$ with 17 equiv of TAIPDI.

In Figure 8, the femtosecond spectra of TAIPDI−$ZnTPPSK_4$ in water display a very rapid formation of broad transient

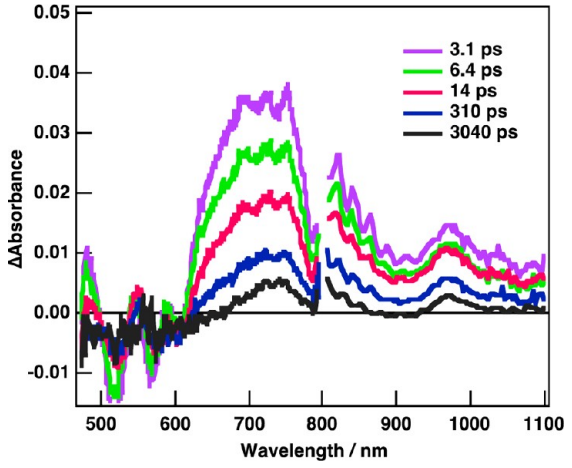

Figure 8. Femtosecond transient absorption spectra of TAIPDI−$ZnTPPSK_4$ in deaerated water at indicated time delays (λ_{exc} = 390 nm).

absorption around 730 and 980 nm. Different than those of singlet-excited states of TAIPDI (vide supra) and $ZnTPPSK_4$[36] in water, these patterns quite match the radical anion of $(TAIPDI)_n$ (Figure S2, Supporting Information),[29] evidence of photoinduced electron transfer from $ZnTPPSK_4$ to $(TAIPDI)_n$. The radical cation of $ZnTPPSK_4$ at 670 nm may have a contribution to the broadening around 700 nm.[44] From the rise at 730 and 980 nm, the rate of charge separation (k_{CS}) is

dx.doi.org/10.1021/jp308549w | J. Phys. Chem. C 2012, 116, 23274−23282

estimated to be 1.4×10^{12} s^{-1} (0.74 ps). Very fast charge separation results from the tight stacking of the donor and acceptor components in the columnar arrays. The time profiles of absorbance at 730 and 980 nm give two-component decay, as shown in Figure 9 and Figure S10 (Supporting Information).

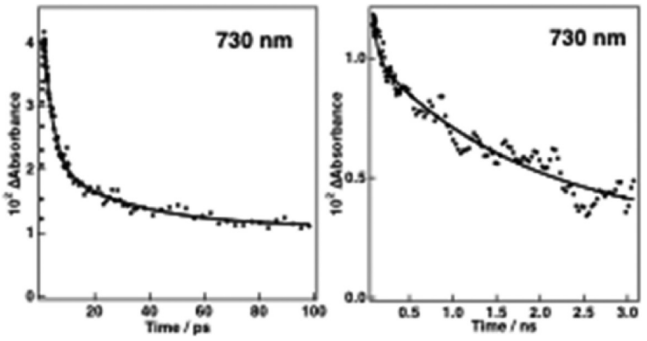

Figure 9. Decay time profiles of the transient absorbance at 730 nm at 0−100 ps (left) and 100−3000 ps (right) in water.

The first component decays with a rate of 2.0×10^{11} s^{-1} (k_{CR1}), yielding a lifetime for first charge recombination as 5 ps (τ_{CS1}) at 730 nm. The second component declines so slowly that it remains incomplete, as observed in all transient traits of $(TAIPDI)_n^{\bullet-}$ in Figure 8. The first-order plot fitted to this slow decay affords a rate constant for second charge recombination as 4.6×10^8 s^{-1} (k_{CR2}), corresponding to 2.2 ns (τ_{CS2}). Such a long-lived charge-separated state is most likely the outcome of the electron transport along the one-dimensional π-stacks of TAIPDI after the photoinduced charge injection occurs. The fast charge recombination correlated with k_{CR1} can be due to the tight stacking. As it facilitates the very fast charge separation, it also causes fast charge recombination due to enhanced electronic communication between the donor and acceptor moieties.[45] Another reason for the first decay component can be the random distribution of the $ZnTPPSK_4$ within the TAIPDI stacks as represented in Figure 10. As a result of this random disposition, there may exist extended domains of TAIPDIs (illustrated as domain 1 in Figure 10) permitting wide-ranging π-electron delocalization, while some domains (illustrated as domain 2 in Figure 10), severed by many $ZnTPPSK_4$ molecules, limit this process favoring the fast recombination. Lastly, stacking defects among the TAIPDI molecules can severely hinder the charge hopping.[46] Despite these drawbacks, almost 3000-times elongated lifetime of the charge-separated state has been ultimately achieved by long-range electron migration through the hydrophobic π-stacks triggered by an aqueous environment. This is the highest k_{CS}/k_{CR} ratio dated for such columnar systems to the best of our knowledge. Nanosecond transient spectra of the TAIPDI−$ZnTPPSK_4$ did not give any signal (Figure S11, Supporting Information), indicating that the charge recombination completed before 100 ns.[47] Absence of the transient signal also proves that the charge-separated state decays directly to the ground state without producing the triplet state of $ZnTPPSK_4$[11g] or TAIPDI,[48] which is already energetically unfeasible. Furthermore, absence of the triplet-excited states of $ZnTPPSK_4$ indicates that $^1ZnTPPSK_4$* is efficiently used for charge injection to the TAIPDI stacks.

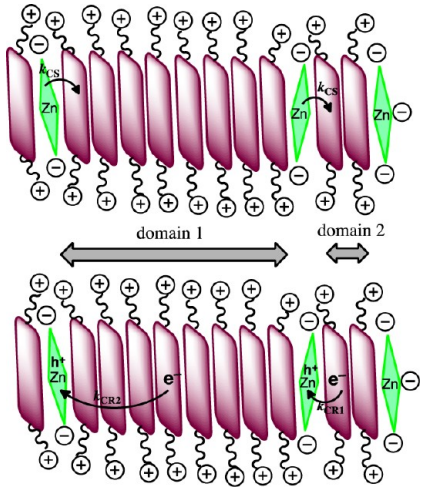

Figure 10. Representative illustration of the charge separation and charge recombination between the stacks of TAIPDI and randomly distributed $ZnTPPSK_4$.

4. CONCLUSION

Columnar TAIPDI stacks at nanoscale have been thoroughly characterized in water and solid state. Excited-state dynamics of $(TAIPDI)_n$ have been explained by a comparison with those of unstacked TAIPDI. The one-dimensional stacks of TAIPDI can host $ZnTPPSK_4$ molecules at various ratios due to strong $\pi-\pi$ and ionic interactions in an aqueous medium. Following the photoinduced charge injection from $ZnTPPSK_4$, electron transport owing to the probable π-delocalization mechanism along the electron deficient TAIPDI stacks has been observed. This phenomenon facilitates the long-range charge separation with a high k_{CS}/k_{CR} ratio, which is a fundamental parameter for organic photovoltaic applications targeting high efficiencies.

■ ASSOCIATED CONTENT

Supporting Information

Figures S1−S11 showing steady-state absorption spectra, DLS diagram, fluorescence and femtosecond absorption decay profiles, cyclic and differential pulse voltammograms, and femtosecond and nanosecond transient absorption spectra. This material is available free of charge via the Internet at http://pubs.acs.org.

■ AUTHOR INFORMATION

Corresponding Author

*E-mail: fukuzumi@chem.eng.osaka-u.ac.jp.

Notes

The authors declare no competing financial interest.

■ ACKNOWLEDGMENTS

This work was supported by a Grant-in-Aid (No. 20108010), and a Global COE program, "the Global Education and Research Center for Bio-Environmental Chemistry" from the Ministry of Education, Culture, Sports, Science and Technology (MEXT), Japan (to S.F.), NRF/MEST of Korea through WCU (R31-2008-000-10010-0) and GRL (2010-00353) Programs. M.S. kindly appreciates Dr. Kenji Saito for helping during the SEM measurements and MEXT, Japan, for a scholarship.

REFERENCES

(1) (a) Marcus, R. A.; Sutin, N. *Biochim. Biophys. Acta* **1985**, *811*, 265−322. (b) Moser, C. C.; Keske, J. M.; Warncke, K.; Farid, R. S.; Dutton, P. L. *Nature* **1992**, *335*, 796−802.

(2) (a) Sariciftci, N. S.; Smilowitz, L.; Heeger, A. J.; Wudl, F. *Science* **1992**, *258*, 1474−1476. (b) Günes, S.; Neugebauer, H.; Sariciftci, N. S. *Chem. Rev.* **2007**, *107*, 1324−1338.

(3) This distance includes all the electron-transfer components in the photosynthetic reaction center. See: Loll, B.; Kern, J.; Saenger, W.; Zouni, A.; Biesiadka, J. *Nature* **2005**, *438*, 1040−1044.

(4) (a) Wasielewski, M. R. *Chem. Rev.* **1992**, *92*, 435−461. (b) Gust, D.; Moore, T. A.; Moore, A. L. *Acc. Chem. Res.* **2001**, *34*, 40−48. (c) Fukuzumi, S. *Phys. Chem. Chem. Phys.* **2008**, *10*, 2283−2297. (d) Fukuzumi, S.; Ohkubo, K. *J. Mater. Chem.* **2012**, *22*, 4575−4587.

(5) (a) Imahori, H.; Guldi, D. M.; Tamaki, K.; Yoshida, Y.; Luo, C.; Sakata, Y.; Fukuzumi, S. *J. Am. Chem. Soc.* **2001**, *123*, 6617−6628. (b) Imahori, H.; Sekiguchi, Y.; Kashiwagi, Y.; Sato, T.; Araki, Y.; Ito, O.; Yamada, H.; Fukuzumi, S. *Chem.—Eur. J.* **2004**, *10*, 3184−3196. (c) Guldi, D. M.; Imahori, H.; Tamaki, K.; Kashiwagi, Y.; Yamada, H.; Sakata, Y.; Fukuzumi, S. *J. Phys. Chem. A* **2004**, *108*, 541−548.

(6) Pivrikas, A.; Neugebauer, H.; Sariciftci, N. S. *Sol. Energy* **2011**, *85*, 1226−1237.

(7) Efficient light funneling in photosynthesis is achieved by an excitation energy-transfer mechanism from specialized light harvesting antenna complexes to the photosynthetic reaction center. Blankenship, R. E. *Molecular Mechanisms of Photosynthesis*; Blackwell Science: Oxford, U.K., 2002.

(8) (a) Brabec, C. J.; Sariciftci, N. S.; Hummelen, J. C. *Adv. Funct. Mater.* **2001**, *11*, 15−26. (b) Coropceanu, V.; Cornil, J.; Filho, D. A. d. S.; Olivier, Y.; Silbey, R.; Bredas, J.-L. *Chem. Rev.* **2007**, *107*, 926−952.

(9) Instead of polymers, small-molecular-weight organic materials, having extensive π-systems, have also been suggested. See: Peumans, P.; Uchida, S.; Forrest, S. R. *Nature* **2003**, *425*, 158−162.

(10) Bakulin, A. A.; Rao, A.; Pavelyev, V. G.; van Loosdrecht, P. H. M.; Pshenichinikov, M. S.; Niedzialek, D.; Cornil, J.; Beljonne, D.; Friend, R. H. *Science* **2012**, *335*, 1340−1344.

(11) (a) Bonvoisin, J.; Launay, J.-P.; Van der Auweraer, M.; De Schryver, F. C. *J. Phys. Chem.* **1994**, *98*, 5052−5057. (b) Bonvoisin, J.; Launay, J.-P.; Verbouwe, W.; Van der Auweraer, M.; De Schryver, F. C. *J. Phys. Chem.* **1996**, *100*, 17079−17082. (c) Nelsen, S. F.; Tran, H. Q.; Nagy, M. A. *J. Am. Chem. Soc.* **1998**, *120*, 298−304. (d) Kochi, J. K.; Rathore, R.; Le Magueres, P. *J. Org. Chem.* **2000**, *65*, 6826−6836. (e) Le Magueres, P.; Lindeman, S. V.; Kochi, J. K. *J. Chem. Soc., Perkin Trans. 2* **2001**, 1180−1185. (f) Onodera, H.; Araki, Y.; Fujitsuka, M.; Onodera, S.; Ito, O.; Bai, F.; Zheng, M.; Yang, J.-L. *J. Phys. Chem. A* **2001**, *105*, 7341−7349. (g) Takai, A.; Gros, C. P.; Barbe, J.-M.; Guilard, R.; Fukuzumi, S. *Chem.—Eur. J.* **2009**, *15*, 3110−3122. (h) Takai, A.; Gros, C. P.; Barbe, J.-M.; Fukuzumi, S. *Chem.—Eur. J.* **2011**, *17*, 3420−3428.

(12) (a) Tanaka, M.; Ohkubo, K.; Gros, C. P.; Guilard, R.; Fukuzumi, S. *J. Am. Chem. Soc.* **2006**, *128*, 14625−14633. (b) Chen, Y.; El-Khouly, M. E.; Zhuang, X.-D.; He, N.; Araki, Y.; Lin, Y.; Ito, O. *Chem.—Eur. J.* **2007**, *13*, 1709−1714. (c) El-Khouly, M. E.; Chen, Y.; Zhuang, X.; Fukuzumi, S. *J. Am. Chem. Soc.* **2009**, *131*, 6370−6371. (d) Fukuzumi, S.; Hanazaki, R.; Kotani, H.; Ohkubo, K. *J. Am. Chem. Soc.* **2010**, *132*, 11002−11003. (e) Takai, A.; Chkounda, M.; Eggenspiller, A.; Gros, C. P.; Lachkar, M.; Barbe, J.-M.; Fukuzumi, S. *J. Am. Chem. Soc.* **2010**, *132*, 4477−4489.

(13) (a) Grimsdale, A. C.; Müllen, K. *Angew. Chem., Int. Ed.* **2005**, *44*, 5592−5629. (b) Weickert, J.; Dunbar, R. B.; Hesse, H. C.; Wiedemann, W.; Schmidt-Mende, L. *Adv. Mater.* **2011**, *23*, 1810−1828.

(14) (a) Hoeben, F. J. M.; Jonkheijm, P.; Meijer, E. W.; Schenning, A. P. H. J. *Chem. Rev.* **2005**, *105*, 1491−1546. (b) Zang, L.; Che, Y.; Moore, J. S. *Acc. Chem. Res.* **2008**, *41*, 1596−1608.

(15) Che, Y.; Datar, A.; Balakrishnan, K.; Zang, L. *J. Am. Chem. Soc.* **2007**, *129*, 7234−7235.

(16) (a) Che, Y.; Datar, A.; Yang, X.; Naddo, T.; Zhao, J.; Zang, L. *J. Am. Chem. Soc.* **2007**, *129*, 6354−6355. (b) Chen, S.-G.; Branz, H. M.; Eaton, S. S.; Taylor, P. C.; Cormier, R. A.; Gregg, B. A. *J. Phys. Chem. B* **2004**, *108*, 17329−17336.

(17) Supur, M.; Yamada, Y.; El-Khouly, M. E.; Honda, T.; Fukuzumi, S. *J. Phys. Chem. C* **2011**, *115*, 15040−15047.

(18) (a) Würthner, F.; Chen, Z.; Hoeben, F. J. M.; Osswald, P.; You, C.-C.; Jonkheijm, P.; Herrikhuyzen, J. v.; Schenning, A. P. H. J.; van der Schoot, P. P. A. M.; Meijer, E. W.; Beckers, E. H. A.; et al. *J. Am. Chem. Soc.* **2004**, *126*, 10611−10618. (b) Sinks, L. E.; Rybtchinski, B.; Iimura, M.; Jones, B. A.; Goshe, A. J.; Zuo, X.; Tiede, D. M.; Li, X.; Wasielewski, M. R. *Chem. Mater.* **2005**, *17*, 6295−6303.

(19) Related reviews: (a) Toksoz, S.; Acar, H.; Guler, M. O. *Soft Matter* **2010**, *6*, 5839−5849. (b) Görl, D.; Zhang, X.; Würthner, F. *Angew. Chem., Int. Ed.* **2012**, *51*, 6328−6348.

(20) Kavarnos, G. J.; Turro, N. J. *Chem. Rev.* **1986**, *86*, 401−449.

(21) Huang, Y.; Quan, B.; Wei, Z.; Liu, G.; Sun, L. *J. Phys. Chem. C* **2009**, *113*, 3929−3933.

(22) Wang, B.; Yu, C. *Angew. Chem., Int. Ed.* **2010**, *49*, 1485−1488.

(23) Jimenez, H. R.; Julve, M.; Faus, J. *J. Chem. Soc., Dalton Trans.* **1991**, 1945−1949.

(24) Iverson, I. K.; Casey, S. M.; Seo, W.; Tam-Chang, S.-W.; Pindzola, B. A. *Langmuir* **2002**, *18*, 3510−3516.

(25) Giaimo, J. M.; Lockard, J. V.; Sinks, L. E.; Scott, A. M.; Wilson, T. M.; Wasielewski, M. R. *J. Phys. Chem. A* **2008**, *112*, 2322−2330.

(26) According to the exciton coupling model, coupling of π-orbital electrons of identical chromophores in cofacial order results in two new exciton states: a higher exciton state, to which the transition from ground state is allowed, and a lower exciton state, to which the transition from ground state is forbidden.[25]

(27) This emission band seems quite different from broad, featureless excimer-like emission, which arises from partial overlap of π-systems as reported earlier for a dimer system.[25]

(28) Aggregation yields have been estimated from the ratio of absolute quantum yield of TAIPDI in water at indicated concentrations to that in MeOH ($\Phi_{f\text{-water}}/\Phi_{f\text{-MeOH}}$). 0.02 mM TAIPDI was assumed to dissolve completely in MeOH. It should be noted that emission originating from TAIPDI stacks at concentrations higher than 0.08 mM can be involved in the quantum yield measurements. However, compared to that of monomer, this emission is very small to cause significant variation of the aggregation values stated in Table 1.

(29) Marcon, R. O.; Brochsztain, S. *J. Phys. Chem. A* **2009**, *113*, 1747−1752.

(30) Shirman, E.; Ustinov, A.; Ben-Shitrit, N.; Weissman, H.; Iron, M. A.; Cohen, R.; Rybtchinski, B. *J. Phys. Chem. B* **2008**, *112*, 8855−8858.

(31) van der Boom, T.; Hayes, R. T.; Zhao, Y.; Bushard, P. J.; Weiss, E. A.; Wasielewski, M. R. *J. Am. Chem. Soc.* **2002**, *124*, 9582−9590.

(32) Size distribution is not correlated with concentration.

(33) (a) Danilov, E. O.; Rachford, A. A.; Goeb, S.; Castellano, F. N. *J. Phys. Chem. A* **2009**, *113*, 5763−5768. (b) Supur, M.; El-Khouly, M. E.; Seok, J. H.; Kim, J. H.; Kay, K.-Y.; Fukuzumi, S. *J. Phys. Chem. C* **2010**, *114*, 10969−10977. (c) Würthner, F. *Chem. Commun.* **2004**, 1564−1579.

(34) Nanostructures are obtained by drop casting of a concentrated TAIPDI aqueous solution (ca. 0.4 mM) onto silicon substrate.

(35) Balakrishnan, K.; Datar, A.; Naddo, T.; Huang, J.; Oitker, R.; Yen, M.; Zhao, J.; Zang, L. *J. Am. Chem. Soc.* **2006**, *128*, 7390−7398.

(36) Supur, M.; Yamada, Y.; Fukuzumi, S. *J. Mater. Chem.* **2012**, *22*, 12547−12552.

(37) According to a 1:1 ratio, the absorbance change is given by the equation $[\text{TAIPDI}]_0/(A_0 - A) = (\varepsilon_c - \varepsilon_p)^{-1} + (K_0[\text{ZnTPPSK}_4](\varepsilon_c - \varepsilon_p))^{-1}$, where A_0 and A are the absorbance of TAIPDI at 501 nm in the absence and presence of ZnTPPSK_4 and ε_c and ε_p are the molar absorption coefficients of TAIPDI at 501 nm in the absence and presence of ZnTPPSK_4, respectively. This equation predicts a linear correlation between $[\text{TAIPDI}]_0/(A - A_0)$ and $[\text{ZnTPPSK}_4]^{-1}$.[38]

(38) (a) Fukuzumi, S.; Kondo, Y.; Mochizuki, S.; Tanaka, T. *J. Chem. Soc., Perkin Trans. 2* **1989**, 1753−1761. (b) Fukuzumi, S.; Amasaki, I.; Ohkubo, K.; Gros, C. P.; Guilard, R.; Barbe, J.-M. *RSC Adv.* **2012**, *2*, 3741−3747.

(39) According to a 1:1 ratio, the absorbance change is given by the equation: $[2{:}3\ \text{complex}]_0/(A_0 - A) = (\varepsilon_c - \varepsilon_p)^{-1} + (K_2[\text{TAIPDI}](\varepsilon_c - \varepsilon_p))^{-1}$, where A_0 and A are the absorbance of 2:3 complex at 430 nm in the absence and presence of TAIPDI and ε_c and ε_p are the molar absorption coefficients of 2:3 complex at 430 nm in the absence and presence of TAIPDI, respectively. This equation predicts a linear correlation between $[2{:}3\ \text{complex}]_0/(A - A_0)$ and $[\text{TAIPDI}]^{-1}$.[38]
(40) It is also likely that TAIPDI stacks have only ionic interactions with $ZnTPPSK_4$ molecules buried in the complex, giving no spectral change.
(41) Weller, A. *Z. Phys. Chem.* **1982**, *133*, 93−98.
(42) Because TAIPDI and $ZnTPPSK_4$ are closely packed in the π-stacks, the initial products of photoinduced electron transfer are assumed to be a contact radical ion pair and ΔG_s was estimated by using the expression $\Delta G_s = -0.56\ \text{eV}\ (1/\varepsilon) + 0.003\ \text{eV}$, where ε is the dielectric constant of water at room temperature. See: Arnold, B. R.; Farid, S.; Goodman, J. L.; Gould, I. R. *J. Am. Chem. Soc.* **1996**, *118*, 5482−5483.
(43) (a) Beljone, D.; Hennebicq, E.; Daniel, C.; Herz, L. M.; Silva, C.; Scholes, G. D.; Hoeben, F. J. M.; Jonkheijm, P.; Schenning, A. P. H. J.; Meskers, S. C. J.; et al. *J. Phys. Chem. B* **2005**, *109*, 10594−10604. (b) Marciniak, H.; Li, X.-Q.; Würthner, F.; Lochbrunner, S. *J. Phys. Chem. A* **2011**, *115*, 648−654.
(44) Ohkubo, K.; Kawashima, Y.; Fukuzumi, S. *Chem. Commun.* **2012**, *48*, 4314.
(45) (a) Ohtani, M.; Fukuzumi, S. *Chem. Commun.* **2009**, 4997−4999. (b) El-Khouly, M. E.; Jaggi, M.; Schmid, B.; Blum, C.; Liu, S.-X.; Decurtins, S.; Ohkubo, K.; Fukuzumi, S. *J. Phys. Chem. C* **2011**, *115*, 8325−8334.
(46) Ide, J.; Mereau, R.; Ducasse, L.; Castet, F.; Olivier, Y.; Martinelli, N.; Cornil, J.; Beljonne, D. *J. Phys. Chem. B* **2011**, *115*, 5593−5603.
(47) The time range between 3 and 100 ns is out of the range of our laser systems.
(48) (a) Ford, W. E.; Kamat, P. V. *J. Phys. Chem.* **1987**, *91*, 6373−6380. (b) Fukuzumi, S.; Ohkubo, K.; Ortiz, J.; Gutierrez, A. M.; Fernandez-Lazaro, F.; Sastre-Santos, A. *J. Phys. Chem. A* **2008**, *112*, 10744−10752.